Hindawi
Mathematical Problems in Engineering
Volume 2022, Article ID 3964417, 9 pages
https://doi.org/10.1155/2022/3964417

Research Article

An Optima Combination Method of Three-Frequency Real-Time Cycle Slip Detection for Non-Normal Ionospheric Variation Data

Yaping Gao, Guo Chen, Xi Chen, Liangliang Ma, Tong Luo, and Dongdong Xue

College of Earth Sciences, Chengdu University of Technology, Chengdu 610059, China

Correspondence should be addressed to Yaping Gao; gaoyaping@cdut.edu.cn

Received 28 February 2022; Accepted 14 March 2022; Published 14 April 2022

Academic Editor: Xinyuan Jiang

Copyright © 2022 Yaping Gao et al. This is an open access article distributed under the Creative Commons Attribution License, which permits unrestricted use, distribution, and reproduction in any medium, provided the original work is properly cited.

Linear combinations of triple-frequency help improve the performance of cycle slip detection for high-precision positioning using a single receiver; however, the position can be easily misjudged under ionospheric scintillation conditions or low sampling rates. We propose a method, which is developed specially for the datasets under ionospheric scintillation conditions or low sampling rates, to detect the triple-frequency cycle slips in real-time based on optimal linear combination coefficients and ionospheric range delay. Detection formulas are derived from the triple-frequency geometry-free code-phase combination, and ionospheric range delay is estimated by the wide lane combination. In addition, the principle used to select an optimal linear phase combination coefficient is derived, and the optimal linear coefficient suitable under high ionospheric activity conditions is provided. Finally, the data collected from self-build stations JYPS and NQ01 are used to test the performance of the method. The results demonstrate that the improved method can be used to detect all combinations of cycle slips in real-time, even under conditions of ionospheric scintillation or a sampling period exceeding 10 s.

1. Introduction

In real-time kinematic applications, due to various disturbing factors such as interruption of signals, a low ratio of signal to noise, and vehicle dynamics, the satellite signals of the Global Navigation Satellite System (GNSS) could temporarily get lost; this phenomenon could lead to the discontinuity of an integral number of cycles in phase measurements. As societies develop, the requirement for high precision in real-time is increasingly growing for positioning and navigation applications. Thus, accurate real-time cycle slip detection (CSD) in data processing is challenging.

At present, there are several studies on CSD for two frequencies. The commonly employed approaches include the higher difference method, ionosphere residual error method [1–4], polynomial fitting, combinations of phase, pseudorange [5], and other methods [6, 7]. All these studies were not suitable for high-frequency real-time data processing.

With the development of GNSS, most of the GNSS receivers can receive triple-frequency observations. Thus, combinations with a longer wavelength, less noise, and fewer influential characters can be formed with triple-frequency observations [8], which is an easy and effective approach for triple-frequency CSD and reparation. The combination of linear original observations presented by Lacy et al. and Zhao et al. [9, 10] and the combination of triple-frequency phase-code presented by [10–13] are proposed to detect cycle slips with high interval observation data. Huang et al. proposed a method for identifying three linearly independent geometry-free combination observations for cycle slip detection [14–16]; however, all the triple-frequency phase and code observation need to be reserved, which complicates the program. To overcome these limitations in current ionospheric processing for triple-frequency CSD, we propose an improved method based on optimal linear combination coefficients and ionospheric range delay, and the relevant detection formula is presented. In addition, an optimal linear phase combination coefficient is derived and

proposed for CSD under high ionospheric activity conditions.

This manuscript is organized as follows: first, the influence of ionospheric variations (IVs) stimulated by sampling rate or ionospheric conditions is analyzed; simultaneously, the limitation of several traditional CSD methods ignoring ionospheric influences is presented and discussed. Subsequently, the detection equation including the correction of IV, as well as the corresponding variance, is derived in detail. Finally, the performance of this improved approach is evaluated with simulated and real observation data, and the results are also verified by Turboedit [17–19]. In addition, the research findings and outlooks are summarized at the end of this study.

2. Materials and Methods

Since the combinations formed with triple-frequency observation have the characters of longer wavelength, less noise, and fewer influential, so the common equations of code and phase combinations is derived in this section.

2.1. Triple-Frequency Linear Code-Phase Combination. The code and carrier phase observations can be expressed as follows:

$$\begin{aligned} P_i &= \rho + k_{1i}I_1 + T + m_i + cd^{rs} + cd_i + \varepsilon_i, \\ \lambda_i\varphi_i &= \rho - k_{1i}I_1 + T + m_i + cd^{rs} + cd_i + \lambda_i N_i + e_i, \end{aligned} \tag{1}$$

where P denotes code observations and ρ refers to the geometric distance between a satellite and a station. The ionospheric delay on L_1 is denoted by I_1. The symbol c refers to the speed of light in vacuum and d^{rs} refers to the clock error difference between satellite s and receiver r. Terms m, d, and T refer to the multipath effect, hardware delay, and tropospheric delay, respectively. ε and e denote the code and phase noise, λ, φ, and N denote the carrier phase wavelength, carrier phase observation, and integer ambiguity, respectively. The symbol $k_{1i} = f_1^2/f_1^2$, where f denotes the signal frequency, and the subscript i ($i = 1, 2, 3$) refers to the signal.

Based on the theory of combination for triple-frequency data, the subscripts f, c, and n are assumed to belong to the integer number field; meanwhile, a, b, and c belong to the real numbers, and $a + b + c = 1$ [20]. Therefore, the triple-frequency carrier phase and code combination observation equations are expressed as follows:

$$P_{abc} = \rho + \beta_{abc}I_1 + T_{abc} + m_{abc} + cd^{rs}_{abc} + cd_{abc} + \varepsilon_{abc}, \tag{2}$$

$$\begin{aligned} \lambda_{lmn}\varphi_{lmn} = \rho - \beta_{lmn}I_1 + T_{lmn} + \lambda_{lmn}m_{lmn} + cd^{rs}_{lmn} + cd_{lmn} \\ + \lambda_{lmn}N_{lmn} + \lambda_{lmn}e_{lmn}, \end{aligned} \tag{3}$$

where P_{abc} and φ_{lmn}, respectively, refer to the code and carrier phase combination observations. $\beta_{abc} = a + bf_1^2/f_2^2 + cf_1^2/f_3^2$ and $\beta_{lmn} = l + mf_1^2/f_2^2 + nf_1^2/f_3^2$ are the amplification factors of ionospheric delay for code and phase, respectively. The subscripts a, b, and c in the equations refer to the linear code combined observations, and l, m, and n refer to the linear phase combined observations.

Based on (2) and (3), N_{lmn} can be obtained as follows:

$$N_{lmn} = \left(\varphi_{lmn} - T_{lmn} - m_{lmn} - e_{lmn} - cd^{rs}_{lmn}\right) - \frac{\left(P_{abc} - T_{abc} - m_{abc} - \varepsilon_{abc} - cd^{rs}_{abc}\right)}{\lambda_{lmn}} + \left(\beta_{lmn} + \beta_{abc}\right)\cdot\frac{I_1}{\lambda_{lmn}} + \frac{c\left(d_{lmn} - d_{abc}\right)}{\lambda_{lmn}}, \tag{4}$$

where $N_{lmn}(k)$ and $N_{lmn}(k-1)$, respectively, are the combined ambiguity in epoch k and $k-1$. The difference between epochs can then be expressed as follows:

$$\begin{aligned} \delta N_{lmn} = N_{lmn}(t_1) - N_{lmn}(t_0) = \left(\delta\varphi_{lmn} - \delta T_{lmn} - \delta m_{lmn} - \delta e_{lmn} - c\delta d^{rs}_{lmn}\right) - \frac{\left(\delta P_{abc} - \delta T_{abc} - \delta m_{abc} - \delta\varepsilon_{abc} - c\delta d^{rs}_{abc}\right)}{\lambda_{lmn}} \\ + \frac{\left(\beta_{lmn} + \beta_{abc}\right)\cdot\delta I_1}{\lambda_{lmn}} + \frac{c\left(\delta d_{lmn} - \delta d_{abc}\right)}{\lambda_{lmn}}, \end{aligned} \tag{5}$$

where the operator δ represents the difference between consecutive epochs k and $k-1$.

Because a few complex modeled errors, such as m, e, and ε, can be possibly minimized by the differencing between consecutive epochs, the troposphere and the clock errors are removed by forming the carrier-minus-code combinations. Therefore, the equation ignoring terms $c\delta d^{rs}$, $c\left(\delta d_{lmn} - \delta d_{abc}\right)$, and δT, δN_{lmn} can be expressed as follows:

$$\delta N_{lmn} = \delta\varphi_{lmn} - \frac{\delta P_{abc}}{\lambda_{lmn}} + \left(\beta_{lmn} + \beta_{abc}\right)\cdot\lambda^{-1}_{lmn}\cdot\delta I_1. \tag{6}$$

In real-time cycle slip detection, the term $\left(\beta_{lmn} + \beta_{abc}\right)\cdot\lambda^{-1}_{lmn}\cdot\delta I_1$ is always ignored because of the small amplification factor of ionospheric delay; however, influences from other factors, such as magnetic storms, may lead to misjudgments in cycle slips in the data preprocessing. Thus, the ionospheric variations should be considered in CSD.

2.2. Geometry-Free Combination. The ionosphere has dispersive characteristics, which is affected by several factors, particularly solar radiation. Thus, the ionospheric activity over the same area will frequently vary with the degree of solar radiation caused by the rotation of the Earth. Commonly, this influence is often ignored or is weakened by ionospheric free combinations; however, owing to the sampling rate or ionosphere activity, the term δI_1 in (6) will change drastically, leading to a possible failure of detection.

In phase observation equation (2), the term N cannot be accurately calculated. It is assumed that the variation of the multipath, observation noise, and hardware delay are relatively stable between consecutive epochs, and clock errors can be removed by geometry-free combination. In addition, the term δI_1 can be obtained with geometry-free observation, and then δI_1 can be expressed as follows:

$$\delta I_1 = \frac{\left(\lambda_i \delta\varphi_i - \lambda_j \delta\varphi_j\right)}{\left(k_{1j} - k_{1i}\right)}. \tag{7}$$

From (7), it can be seen the ionospheric variation could be derived from carrier phase observations between consecutive epochs.

2.3. Formula of Triple-Frequency Cycle Slip Detection. As outlined above, with different levels of activity in the ionosphere or sampling rate, ionospheric variations between epochs will near normal distribution. Thus, the statistical law for CSD $N(\delta N_{ijk}, \sigma^2_{\delta N_{ijk}})$ will be ineffective under those conditions. So, the ionospheric variation should be considered in (6), and the algorithm proof can be expressed as follows:

$$\delta N_{lmn} = \delta\varphi_{lmn} - \frac{\delta P_{abc}}{\lambda_{lmn}} + K \cdot \left(\lambda_i \delta\varphi_i - \lambda_j \delta\varphi_j\right), \tag{8}$$

where $K = (k_{1j} - k_{1i})^{-1} \cdot (\beta_{lmn} + \beta_{abc}) \cdot \lambda_{lmn}^{-1}$.

Applying the variance-covariance propagation law, the variance σ of δN_{lmn} can be obtained as follows:

$$\sigma_{\delta N_{lmn}} = \sqrt{2\left[\left(i^2 + j^2 + k^2\right)\sigma_\varphi^2 + \lambda_{lmn}^{-2} \cdot \sigma_{abc}^2\right] + K^2 \cdot 2\left(\lambda_i^2 + \lambda_j^2\right)\sigma_\varphi^2}. \tag{9}$$

From (9), we assume $\sigma_{P_1} = \sigma_{P_2} = \sigma_{P_3} = 0.3$ m, $\sigma_{L_1} = \sigma_{L_2} = \sigma_{L_3} = 0.01$ cycles, and the respective carrier wavelengths are $\lambda_1 \approx 19.03$ cm, $\lambda_2 \approx 24.42$ cm, and $\lambda_3 \approx 25.48$ cm. If we select $abc = [1, 0, 0]$, it can be known from (9)that the variance of δN_{lmn} depends on σ_P.

The probability of successfully detecting the triple-frequency cycle slip is

$$\left|\delta N_{lmn}\right| > l \cdot \sigma_{\delta N_{lmn}}, \tag{10}$$

where $l = 3, 4$ (where the respective confidence levels are 99.7% and 99.9%). When $|\delta N_{lmn}| > l \cdot \sigma_{\delta N_{lmn}}$, a cycle slip is found.

It can be seen from (10), the variance of δN_{lmn} is not only dependent on the noise of the code observations but also on the optimum phase combination coefficients to decide whether the observation is cycle slip or not. With a confidence level of 99.9%, it can be noted that the cycle slips within 1 cycle should be detected and ambiguity should be set as a new one. It can be noted that the equation only needs the code and phase observations of current epoch, so it can be used for real-time data processing with any sampling interval.

2.4. Optimum Phase Combination Coefficient. The combination wavelength and combination noise are affected by combination coefficients. Huang et al. investigated such optimal triple-frequency combinations systematically [21,22]. A few linear combinations are listed in Table 1, as well as their corresponding combined wavelengths. The respective variances of δN_{lmn}, eliminating ionospheric variations derived from the dual-frequency combination, are also listed.

Table 1 shows that all $\sigma_{\delta N_{lmn}}$ are within 0.18 cycles.

To select the appropriate combination of phase observations, we formulate a few rules: (1) the influence of the ionosphere should be eliminated or weakened maximally; (2) noise from the troposphere and multipath will not be enlarged. From (5), because all the coefficients of parameters except for that of the ionosphere are consistent, we assume that the ionospheric variation is derived by $\sigma_{\delta N_{lmn}}$. Then, from equations (5) and (6), it can be determined that, if the terms l, m, and n are satisfied with $l \cdot n < 0$ and $|l| \cong |n|$, the combination will be optimum. A noise STD (δN_{lmn}) calculated with IGS normal observation with the combinations listed in Table 1 is given in Figure 1.

Figure 1 shows that the combinations (−3, 1, 3), (3, 0, −4), and (−6, 1, 7) are comparatively optimum, and the STD of δN_{lmn} of combination (−6, 1, 7) is the lowest combination. Therefore, this combination will be used for data processing and analysis.

3. Results and Discussion

The processed combinations of phase observations l, m, and n are set as $[-6, 1, 7]$, and that of the code observation a, b, and c is set as $[1, 0, 0]$. The GPS observations are assumed to have realistic noise of $\sigma_{P_1} = \sigma_{P_2} = \sigma_{P_3} = 0.3$ m and $\sigma_\varphi = 0.01$ cycle. The triple-frequency GPS data from IGS station JFNG are processed to evaluate the performance of our method. The data interval is 1 s, and the cut-off elevations are set as 10°. The data of DOY 211 in 2015 (August 9, 2015) are processed in Sections (1), (2), and (4), and the 76th (March 17, 2015) data are processed in Section (3); the real data collected from self-build station NQ01 and JYPS on January 1, 2017, are also used in Section (5).

3.1. Performance of Conventional Methods. To analyze the characteristics of ionospheric variations derived from different sampling rata, we collected the data under quiet ionospheric activity conditions from JFNG tracking station of an international GPS service (IGS), and the δI_1 values of 1 s and 30 s observation intervals are computed by (7).

Figure 2 shows a typical and practical example of the effect of δI_1, which is based on 1 s with an STD of 0.00124 m

Table 1: Linear combination of triple-frequency and combined wavelengths, and the respective variance of δN_{lmn} with different double-frequency combinations.

Number	(l, m, n)	Turtles	$\sigma_{\delta N_{lmn}}$/cycles		
			$(i = 1, j = 2)$	$(i = 1, j = 3)$	$(i = 2, j = 3)$
1	(7, −8, −1)	9.768	0.15	0.15	0.08
2	(4, −8, 3)	29.305	0.13	0.13	0.13
3	(−6, 1, 7)	29.305	0.13	0.13	0.13
4	(0, 1, −1)	5.861	0.05	0.05	0.05
5	(−4, 9, −4)	7.326	0.16	0.16	0.17
6	(−3, 1, 3)	9.768	0.07	0.07	0.08
7	(−2, −7, 10)	14.653	0.18	0.18	0.18
8	(−1, 8, −7)	29.305	0.15	0.15	0.15
9	(1, −7, 6)	7.326	0.14	0.14	0.14
10	(3, 0, −4)	14.653	0.07	0.07	0.07

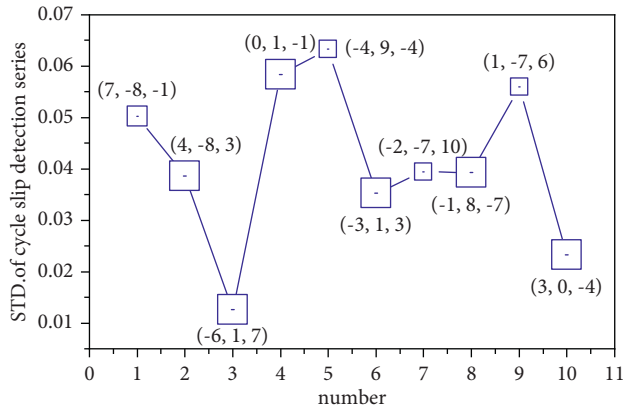

Figure 1: STDs of δN_{lmn} are derived with all combinations listed in Table 1.

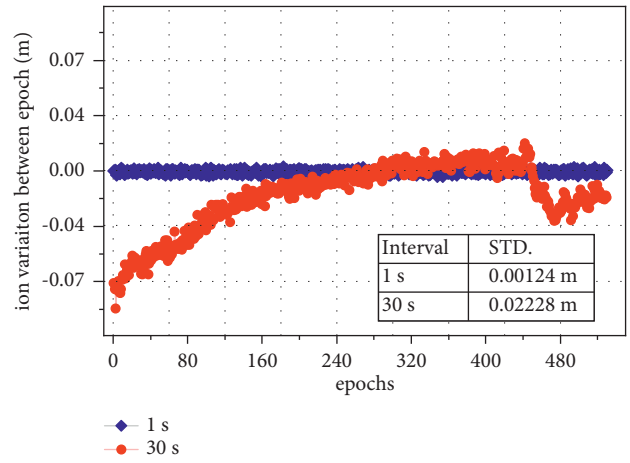

Figure 2: Sequences of ionospheric delay variations in 1 s and 30 s observation intervals. Station: JFNG (China). Receiver/antenna: TRIMBLE NETR9/TRM59800.00. Day: August 9, 2015.

and 30 s with an STD of 0.02228 m dual-frequency GPS data obtained from the IGS station located in China. The receiver and antenna placed at JFNG are TRIMBLE NETR9 and TRM59800.00, respectively. The data correspond to August 9, 2015. Figure 2 clearly shows that δI_1 in 1 s is distributed on both sides of zero, while that at 30 s is observably different. The corresponding histograms are shown in Figure 3. δI_1 at $1 - s$ indicates a normal distribution with a mean of zero; simultaneously, the values at 30 s indicate the high impact of the ionospheric effect.

To further verify the connection between the noise STD of δI and the observation interval, the ionospheric variations of δI at different observation intervals are computed at 1 s, 5 s, 10 s, 15 s, 20 s, 25 s, and 30 s. The corresponding noise STD is presented in Figure 4. The figure shows that the noise STD of δI becomes larger with the increase in the sampling rate. Therefore, the influence of the ionospheric variation should be necessarily considered in cycle slip detection by (6).

It is well known that violent solar activity often causes disturbances in the magnetic field, which is known as a magnetic storm. Under the activity conditions of magnetic storms, the ionospheric variation will be strongly affected, and the CSD will also likely be invalid. A large magnetic storm occurred near the tracking station IGS-JFNG on March 17, 2013. The ionospheric variations on March 17, 2013, and a comparison on the same day in 2014 are shown in Figure 5.

Figure 5 shows that the CSD threshold is 0.08 and that many epochs less than −0.08 will be misjudged beyond the threshold as the cycle jumps; however, they are actually stimulated by ionospheric variations.

3.2. Analysis of CSD with Different Sampling Period Rate Observations. To evaluate the performance of the method with triple-frequency data in different intervals, we sampled the data from IGS-JFNG on August 9, 2015, at 1 s, 5 s, 10 s, 15 s, 20 s, 25 s, and 30 s. The artificial jump (0, 1, 0) is added to all satellite insights, and the ionospheric variation is derived by $f_1 f_3$. The method that is corrected with δI_1 and that without is, respectively, marked in red and blue, and the results are shown in Figure 6 and Table 2.

Because the epochs and amplitudes of the jumps are previously known, as shown in Figure 6, with the increase in sampling rate, the performance of the method when the detection value δI_1 is ignored worsens such that two epochs are missing and five epochs are misjudged. However, all the jumps added artificially are correctly detected with the

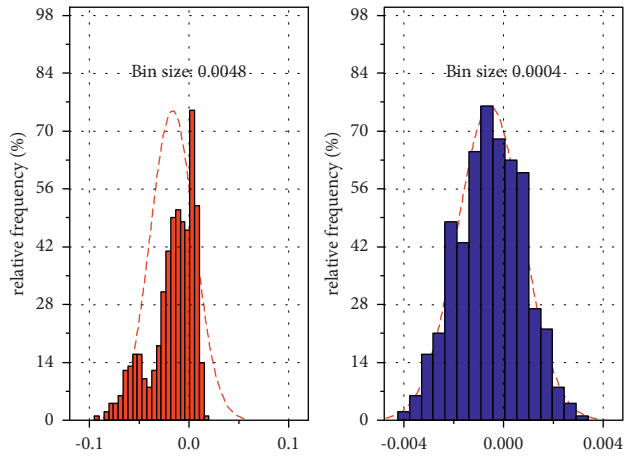

Figure 3: Histogram of the frequency distribution of ionospheric variations from Figure 1.

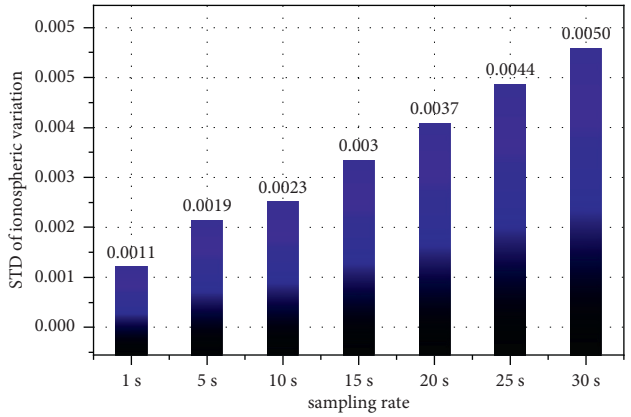

Figure 4: Noise STD of δI at different observation sampling rates.

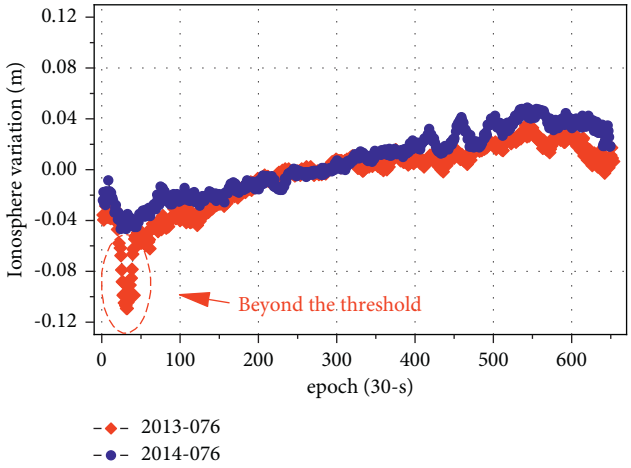

Figure 5: Comparison of the ionospheric variation of geomagnetic storms on March 17, 2013, and that on the same day in 2014.

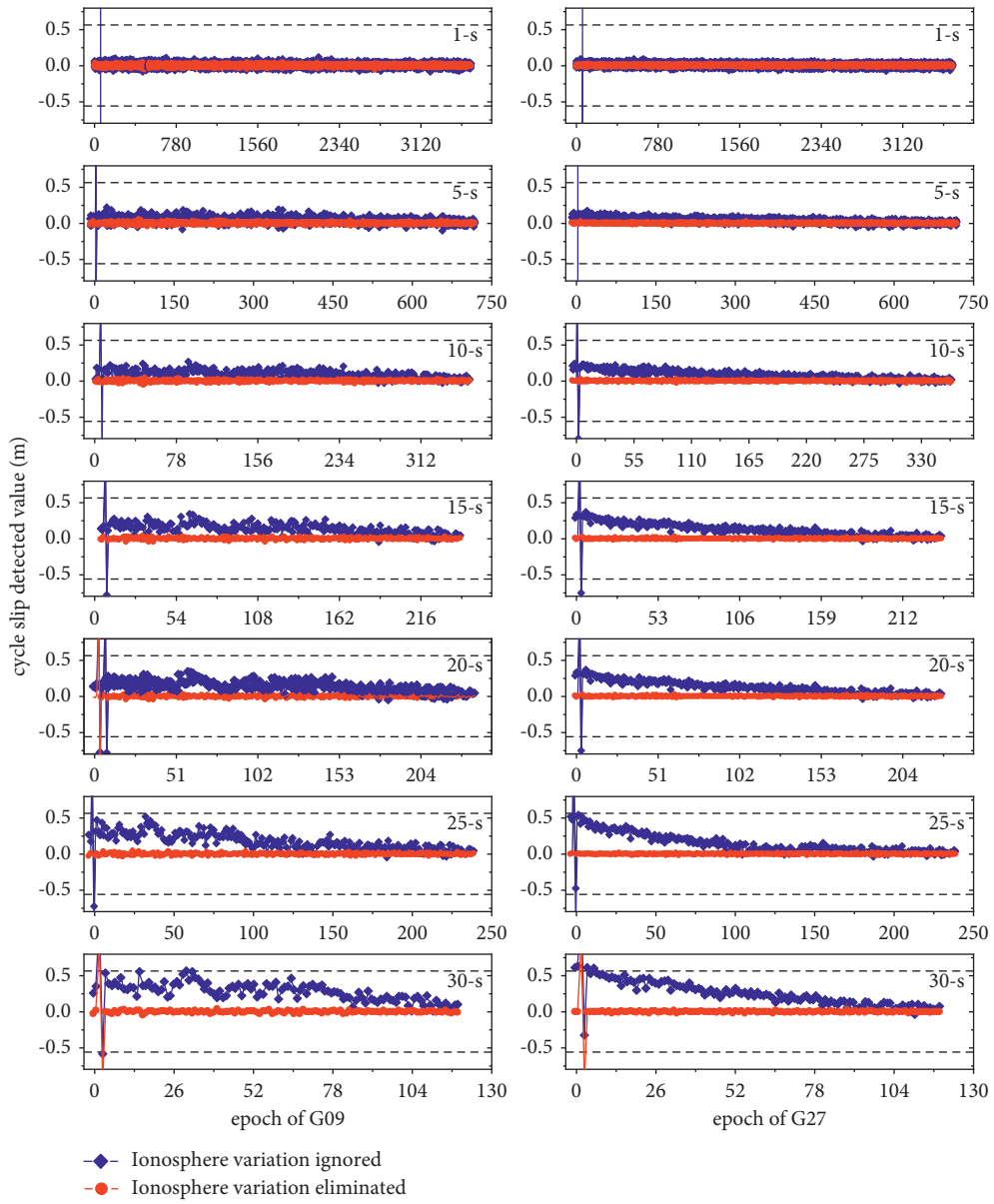

Figure 6: Comparison of CSDs with (blue) or without (red) the ionospheric variations. Different sampling intervals at JFNG equipped with the TRIMBLE NETR9 and G09 (left) and G27 (right) satellites.

improved method, and the detection value is approximately normally distributed on both sides of the x-axis.

3.3. Analysis of Cycle Slip Detection with Ionospheric Scintillation Observations. The analysis above shows that the expectancy of the ionospheric variation δI_1 is not affected by the sampling rate; however, the expectancy is also influenced by the activity of the ionosphere. To further evaluate the performance of the method under the activity of the ionospheric conditions, the data collected at IGS-JFNG (March 17, 2013) under a magnetic storm are considered for processing. The time is 00 : 00 on the 76th day of 2013, JFNG station is located near the center of the magnetic storm, the artificial cycle slips (0, 1, 0) are added on G25, and the sequence of δN_{lmn} and the comparison sequence of the ignored δI_1 are computed, as shown in Figure 7.

Figure 7 shows that the artificial jumps are clearly detected by both methods whether δI_1 is ignored or not; however, almost half of the epochs of δN_{lmn} are marked as jumps by the rules of $4\sigma_{\delta N_{lmn}}$ resulting in the removal of a large number of useful data samples that have been misjudged. It is unlikely that the approach corrected the ionospheric effect with δI_1 and not only detected the artificial jumps correctly but also utilized all data.

3.4. Cycle Slip Detection with an Insensitive Simulation. Sensitive combinations of cycle slips listed in Table 3 are added to the pure data above, and then the data from IGS-

Table 2: Detection results of artificial cycle slips combinations.

True epoch	Sampling rate (s)	Estimated epoch	Detection values (>0.52) (m) ($4\cdot\sigma_{\delta N_{lmn}}$)		Comparison result class
			Without δI_1	With δI_1	
60	1	60	0.999 (G09), 1.008 (G27)	1.000 (G09), 1.001 (G27)	Consistent
12	5	12	1.072 (G09), 1.025 (G27)	1.149 (G09), 0.989 (G27)	Consistent
6	15	6	1.166 (G09), 1.258 (G27)	1.011 (G09), 0.998 (G27)	Consistent
4	20	4	1.180 (G09), 1.322 (G27)	0.998 (G09), 0.996 (G27)	Consistent
3	25	3	−0.722 (G09), −0.476 (G27)	−0.982 (G09), 1.030 (G27)	Consistent
4	25	4	−0.476 (G09)	−0.982 (G09)	Missing
✗	25	5	0.533 (G27)	0.002 (G27)	Misjudgment
✗	25	6	0.549 (G27)	0.006 (G27)	Misjudgment
3	30	3	1.327 (G09), 1.568 (G27)	1.012 (G09), 0.976 (G27)	Consistent
4	30	4	−0.326 (G27)	−1.001 (G27)	Missing
✗	30	5	0.544 (G09), 0.613 (G27)	−0.000 (G09), 0.001 (G27)	Misjudgment
✗	30	16	0.554 (G09)	0.019 (G09)	Misjudgment
✗	30	31	0.563 (G09)	0.014 (G09)	Misjudgment

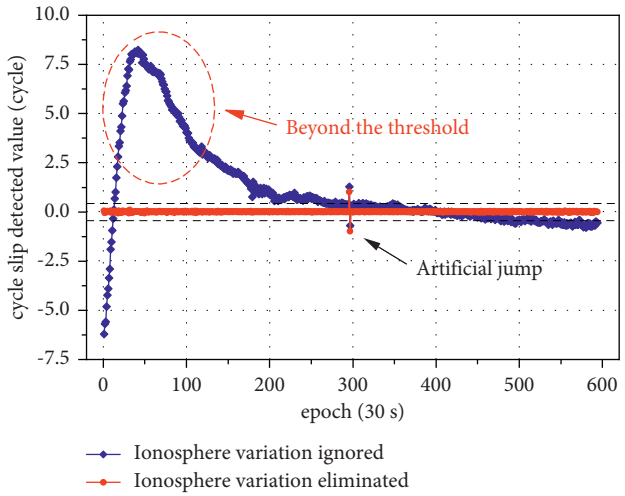

Figure 7: Detection of cycle slips with the data collected in sessions with magnetic storms.

Table 3: Sensitive combinations of cycle slips added and the detected results.

Number	True value	$\lvert\delta N_{lmn}\rvert$ ($>4\cdot\sigma_{\delta N_{lmn}}$)			Yes/No
		f_1f_2 (0.52)	f_1f_3 (0.52)	f_2f_3 (0.52)	
1	(1,0,0)	1.171	0.122	5.838	✓
2	(1,1,0)	7.021	0.884	35.831	✓
3	(1,0,1)	8.227	0.973	41.650	✓
4	(0,1,1)	1.290	0.130	6.407	✓
5	(0,1,0)	8.295	0.963	41.895	✓
6	(0,0,1)	7.065	0.870	35.953	✓
7	(2,3,5)	12.577	1.611	64.340	✓
8	(1,1,1)	0.042	0.001	0.182	✗
9	(9,9,9)	0.354	0.053	1.849	✓
10	(50,50,50)	2.101	0.332	11.90	✓

JFNG on August 9, 2015, are processed using the proposed method. The result demonstrates that all the sensitive combinations except for (1, 1, 1) are detected. Further tests from numbers 8-9 show that, in the same cycle slips, fewer than nine cycles jumped on each frequency and could hardly be detected; we will focus on the reasons for this in future work.

3.5. Cycle Slip Detection with Measurement Data. To further evaluate the performance of our method with real data, triple-frequency data collected from self-build stations NQ01 and JYPS are processed, and the results are shown in Figure 8 and Table 4.

It can be seen from Figure 8 and Table 4 that a few possible jumps can be found at 09 : 39 : 00 (G03), 00 : 39 : 30

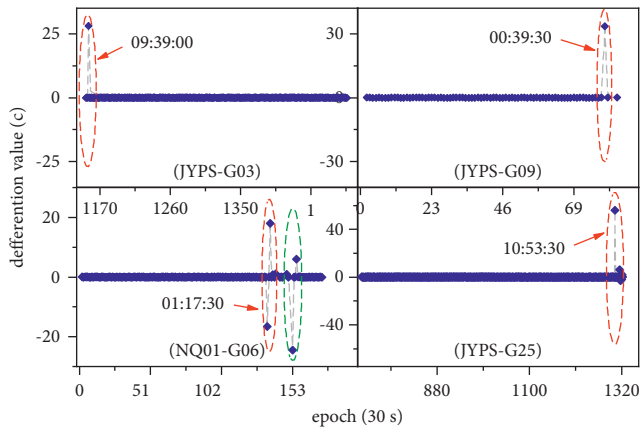

Figure 8: Detecting results with real observation data from iGMAS JYPS and NQ01.

Table 4: Results detected by Turboedit.

Number	PRN	Epoch	Time	Flag	Station
1	G09	80	00 : 39 : 30	DEL	JYPS
2	G03	1155	09 : 39 : 00	DEL	JYPS
3	G25	1308	10 : 53 : 30	DEL	NQ01
4	G06	138	01 : 17 : 30	DEL	NQ01

(G09), and 10 : 53 : 30 (G25) in JYPS and at 01 : 17 : 30 (G06) in NQ01. All the results are shown in Figure 8. The data are also processed by Turboedit, which is known for data preprocessing, and the result is summarized in Table 4. The results are consistent. In addition, the proposed method detects one more jump at the 151st epoch on G06 in NQ01 than Turboedit does.

4. Conclusions

A cycle slip detection method based on triple-frequency combinations and ionospheric variations derived from two consecutive epochs is proposed for triple-frequency CSD without the limitations of sampling rate or ionospheric conditions. A few conclusions can be drawn as follows:

(1) Processed with the data sampled into different intervals or collected near the center of a magnetic storm, the sequence of δI_1 no longer approximately satisfies a normal Gaussian distribution. Together with the advantages of a combination of observations with triple-frequency data, ionospheric variations can be eliminated from δN by δI_1 derived from dual-frequency phase observations, such that the improved value of δN can be reasonably used for CSD.

(2) Because the noise STD δI_1 is based on frequency, the series of δI_1 derived from $f_1 f_2$, $f_1 f_3$, and $f_2 f_3$ are statistically analyzed. Subsequently, three different δI_1 values are corrected from δN in the cycle slip detection process. The result notes that some small cycle slips, even within less than 0.05 cycles, can be detected by the improved δN-corrected δI_1 with appropriate frequency combinations.

(3) To evaluate the performance of our method, we processed with data from different sampling rates and under the conditions of high ionospheric activity. The results demonstrate that all the artificially added cycle slips are detected using the detection value δN without misjudging or missing any of the cycle slips; moreover, most of the sensitive cycle slips are detected as well.

(4) In this study, the real measured data are also applied to evaluate the performance of the approach. Simultaneously, the software Turboedit is adopted for comparison. The comparative results indicate that the proposed method performs better than Turboedit does when more jumps are detected in the real-time data.

To summarize, the proposed algorithm can be easily and effectively implemented for cycle slip detection with triple-frequency data. Nevertheless, there are still a few issues, such as the detection of the cycle slip combination (1,1,1) in Table 3 and the repair of cycle slips, that we intend to focus on our future work.

Data Availability

The raw and processed data required to reproduce these findings cannot be shared at this time as the data also form part of an ongoing study.

Conflicts of Interest

The authors declare that there are no conflicts of interest regarding the publication of this paper.

Acknowledgments

The authors would like to acknowledge the voluntary participation of all the subjects during the study. Additionally, the authors thank IGS for providing triple-frequency GPS data. The authors thanks Professor Rui Tu from the Time Service Center of the Chinese Academy of Sciences for the technical guidance provided to this article. This work was supported by Applied Basic Research Project of Sichuan

Provincial Department of Science and Technology (grant no. 2020YJ0362) and Sichuan Society of Surveying, Mapping and Geographic Information (grant no. CCX202114).

References

[1] E. Astafyeva, L. Rolland, and P. Lognonné, "Parameters of seismic source as deduced from 1 Hz ionospheric GPS data: case study of the 2011 Tohoku-oki event," *Journal of Geophysical Research: Space Physics*, vol. 118, no. 9, pp. 5942–5950, 2013.

[2] G. Blewitt, "An automatic editing algorithm for GPS data," *Geophysical Research Letters*, vol. 17, pp. 199–202, 2013.

[3] C. Cai, Z. Liu, P. Xia, and W. Dai, "Cycle slip detection and repair for undifferenced GPS observations under high ionospheric activity," *GPS Solutions*, vol. 17, no. 2, pp. 247–260, 2013.

[4] L. Y. Huang and L. V. Zhi-Ping, "Analysis on triple-frequency BDS ionospheric delay correction," *Science Surveying and Mapping*, vol. 40, no. 3, pp. 12–15, 2015.

[5] A. Krypiak-Gregorczyk and P. Wielgosz, "Carrier phase bias estimation of geometry-free linear combination of GNSS signals for ionospheric TEC modeling," *GPS Solutions*, vol. 22, no. 2, pp. 45–62, 2018.

[6] M. C. de Lacy, M. Reguzzoni, and F. Sansò, "Real-time cycle slip detection in triple-frequency GNSS," *GPS Solutions*, vol. 16, no. 3, pp. 353–362, 2012.

[7] B. Li, "Theory and method of parameter estimation for mixed integer GNSS function and stochastic models," *Acta Geodaetica et Cartographica Sinica*, vol. 39, no. 3, p. 330, 2010.

[8] J. Li, Y. Yang, H. He, and J. Xu, "Optimal carrier-phase combinations for triple-frequency GNSS derived from an analytical method," *Acta Geodaetica et Cartographica Sinica*, vol. 41, no. 6, pp. 797–803, 2012.

[9] W. Liu, X. Jin, M. Wu, J. Hu, and Y. Wu, "A new real-time cycle slip detection and repair method under high ionospheric activity for a triple-frequency GPS/BDS receiver," *Sensors*, vol. 18, no. 2, p. 427, 2018.

[10] Z. Liu, "A new automated cycle slip detection and repair method for a single dual-frequency GPS receiver," *Journal of Geodesy*, vol. 85, no. 3, pp. 171–183, 2011.

[11] Z. Ren, L. Li, Z. Jie, M. Zhao, and Y. Shen, "A Real-Time Cycle-Slip Detection and Repair Method for Single Frequency GPS Receiver," in *Proceedings of the 2011 2nd International Conference on Networking and Information Technology*, Singapore, 2011.

[12] Z. Tian, L. Sui, Y. Xu, and X. Jia, "Real-time triple-frequency cycle slip detection and repair method under ionospheric disturbance validated with BDS data," *GPS Solutions*, vol. 22, no. 3, p. 62, 2018.

[13] H. Wei, X. Zhang, Z. Zhang, Y. Li, and R. Pang, "Real-time detection and repair of cycle slips in triple-frequency BDS measurements," *China Satellite Navigation Conference*, vol. III, pp. 429–441, 2017.

[14] K. Younsil, S. Junesol, K. Changdon, and P. Byungwoon, "GPS cycle slip detection considering satellite geometry based on TDCP/INS integrated navigation," *Sensors*, vol. 15, no. 10, pp. 25336–25365, 2015.

[15] L. Dong, Y. Yuan, H. Wang, and Y. Wang, "On an optimum selection method of gps triple-frequency phase combination applied to undifferenced cycle slip detection," *Journal of Geodesy and Geodynamics*, vol. 32, no. 3, pp. 106–105, 2012.

[16] X. Zhang, Q. Zeng, J. He, and C. Kang, "Improving turboedit real-time cycle slip detection by the construction of threshold model," *Geomatics and Information Science of Wuhan University*, vol. 42, no. 3, pp. 285–292, 2017.

[17] Q. Zhang and Q. Gui, "Bayesian methods for outliers detection in GNSS time series," *Journal of Geodesy*, vol. 87, no. 7, pp. 609–627, 2013.

[18] Q. Chen, H Chen, W. Jiang, X. Zhou, and P. Yuan, "A new cycle slip detection and repair method for single-frequency gnss data," *Journal of Navigation*, vol. 71, no. 06, pp. 1–19, 2018.

[19] X. Zhang, F. Guo, and P. Zhou, "Improved precise point positioning in the presence of ionospheric scintillation," *GPS Solutions*, vol. 18, no. 1, pp. 51–60, 2014.

[20] X. Zhang and P. Li, "Benefits of the third frequency signal on cycle slip correction," *GPS Solutions*, vol. 20, no. 3, pp. 451–460, 2016.

[21] Q. Zhao, B. Sun, Z. Dai, C. Shi, and J. Liu, "Real-time detection and repair of cycle slips in triple-frequency GNSS measurements," *GPS Solutions*, vol. 19, no. 3, pp. 381–391, 2015.

[22] B. D. L. Opperman, P. J. Cilliers, L.-A. Mckinnell, and R. Haggard, "Development of a regional GPS-based ionospheric TEC model for South Africa," *Advances in Space Research*, vol. 39, no. 5, pp. 808–815, 2007.